Polymer Chemistry

Accepted Manuscript

ROYAL SOCIETY OF CHEMISTRY

www.rsc.org/polymers

Chemistry of aromatic polythioesters and polydithioesters†

Daisuke Abe, Yuichiro Fukuda and Yuji Sasanuma*

Received Xth XXXXXXXXXX 20XX, Accepted Xth XXXXXXXXX 20XX
First published on the web Xth XXXXXXXXXX 200X
DOI: 10.1039/b000000x

Aromatic polythioesters (abbreviated as PyTS$_2$) and polydithioesters (PyTS$_4$) (y: the number of methylene units = 2 − 5), analogues of the common aromatic polyesters such as poly(ethylene terephthalate) and poly(butylene terephthalate), have been synthesized and characterized in terms of solubility, crystallinity, glass transition, melting, thermal decomposition, molecular motion, and thermal transition. Conformational characteristics of the S−(CH$_2$)$_y$−S bond sequences of the two groups of polymers were investigated through NMR and single crystal X-ray diffraction experiments as well as molecular orbital calculations for their model compounds. The synthetic scheme developed previously for P2TS$_4$ has been successfully extended to its higher homologues, PyTS$_4$ (y = 3 − 5). The structure of the monomer, tetrathioterephthalate acid (S$_4$TPA) complexed with piperidinium (Pip), was determined, and the molar ratio of S$_4$TPA : Pip was evaluated as 1:2 from elemental analysis and density functional theoretical simulations for its ^{1}H and ^{13}C NMR spectra. Two polydithioesters, P3TS$_4$ and P4TS$_4$, show an endothermic change around 130 − 150 °C. By X-ray diffraction and solid state NMR experiments, the endotherm was proved to be due to an irreversible crystalline-to-amorphous transition.

1 Introduction

The common aromatic polyesters (Fig. 1a), poly(ethylene terephthalate) (PET, y = 2), poly(trimethylene terephthalate) (PTT, y = 3), and poly(butylene terephthalate) (PBT, y = 4), were developed at the early stage of polymer industries and have become indispensable materials for industrial applications and our daily lives.[1] The only difference in primary structure between these polyesters is the number (y) of methylene groups in the spacer (−O(CH$_2$)$_y$O−). The crystal structures are formed and stabilized with the aid of intermolecular $\pi - \pi$ attraction between the benzene rings, and the spacer is forced to fill the crystalline space effectively with preserving its inherent conformational preference. As a consequence, their crystalline moduli along the chain axis differ sizably from each other:[2] PET, 110±10 GPa (ttt);[3] PTT, 2.6 GPa (tggt);[4–6] α-form of PBT, 10 − 13 GPa (g$^+$g$^+$tg$^-$g$^-$),[7,8] where the spacer conformation in the crystal is written in the parenthesis. The mechanical properties may essentially determine the practical applications: rigidity of PET, fiber, films, and bottles; elasticity of PTT, sportswear and innerwear; impact residence of PBT, automotive and electric parts.[1] Their structures and properties depend largely on the spacer conformation, *i.e.*, the number of methylene units.

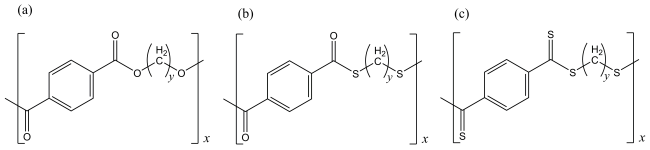

Fig. 1 Chemical structures of aromatic (a) polyesters, (b) polythioesters (PyTS$_2$), and (c) polydithioesters (PyTS$_4$), where y is the number of methylene units in the spacer.

The analogues of the aromatic polyesters, containing two (Fig. 1b) and four (Fig. 1c) sulfur atoms in place of oxygen, are termed polythioesters (PyTS$_2$) and polydithioesters (PyTS$_4$), respectively. In early studies,[9–11] the aromatic polythioester, *e.g.*, P2TS$_2$, P4TS$_2$, P5TS$_2$, and P10TS$_2$, were synthesized from terephthaloyl chloride and aliphatic dithiols, and their melting points and inherent viscosities were measured; however, no detailed characterization has been performed yet.

In a previous study,[12] we predicted structures and properties of these sulfur-containing polymers of y = 2, *viz.*, poly(ethylene dithioterephthalate) (P2TS$_2$) and poly(ethylene tetrathioterephthalate) (P2TS$_4$) from not only *ab initio* molecular orbital (MO) and statistical mechanical calculations but also NMR and single crystal X-ray diffraction experiments for their model compounds and, furthermore, actually synthesized and characterized the two polymers to verify the theoretical predictions. Then, we developed a novel scheme to synthesize

† Electronic Supplementary Information (ESI) available: Optimized S$_4$TPA-Pip structure (Fig. S1); solid state ^{13}C CP/MAS NMR spectra of PyTS$_2$ (Fig. S2) and PyTS$_4$ (Fig. S3); DSC charts of PyTS$_2$ (Fig. S4) and PyTS$_4$ (Fig. S5); Photographs of P3TS$_4$ and P4TS$_4$ powders (Fig. S6). See DOI: 10.1039/b000000x/

Department of Applied Chemistry and Biotechnology, Graduate School and Faculty of Engineering, Chiba University, 1-33 Yayoi-cho, Inage-ku, Chiba 263-8522, Japan. E-mail: sasanuma@faculty.chiba-u.jp; Fax: +81-43-290-3394; Tel: +81-43-290-3394

P2TS$_4$. In the present study, we have extended the synthetic method to PyTS$_4$ of y = 3 − 5 to confirm its broad applicability. The monomer is a complex of tetrathioterephthalate acid and piperidinium (abbreviated herein as S$_4$TPA-Pip). The structure of the complex was investigated by MO calculations, NMR experiments, and elemental analysis. The two groups of polymers, PyTS$_2$ and PyTS$_4$ (y = 3 − 5), were synthesized and characterized by a variety of experimental techniques in terms of solubility, crystallinity, glass transition, melting, thermal decomposition, molecular motion, and thermal transition.

2 Methods

2.1 Synthesis of *S,S'*-(propane-1,3-diyl) dibenzothioate-^{13}C (3DBS$_2$-^{13}C)

Benzoyl chloride (24.0 g, 170 mmol) was added dropwise to anhydrous pyridine (13.6 g, 170 mmol) and 1,3-propapedithiol (26.0g, 340 mmol) kept at 0 °C and then stirred at room temperature for 4 h. The reaction mixture was diluted with diethyl ether and washed with water twice. The organic layer was evaporated and distilled at 150 °C and 1 mmHg to collect the crude product, which was distilled again at 70 °C and 2 mmHg to remove 1,3-propanedithiol completely. The residue was *S*-(3-melcaptopropyl)benzothioate (20.0 g, 55%).

Benzoyl-*carbonyl*-^{13}C chloride (0.51 g, 3.6 mmol) was added to anhydrous pyridine (0.28 g, 3.6 mmol) and *S*-(3-melcaptopropyl)benzothioate (1.1 g, 5.2 mmol) and stirred at room temperature for 45 h. The reaction mixture was diluted with diethyl ether, washed with water twice, and the organic layer was evaporated. The residue was recrystallized from ethanol twice to yield 3DBS$_2$-^{13}C (0.11 g, 10%).

2.2 Synthesis of propane-1,3-diyl dibenzodithioate-^{13}C (3DBS$_4$-^{13}C)

S,S'-(Propane-1,3-diyl) dibenzothioate-^{13}C (3DBS$_2$-^{13}C, 0.06 g, 0.19 mmol) and Lawesson's reagent (0.09 g, 0.22 mmol) were added to anhydrous xylene (20 mL) and stirred at 140 °C for 3 h.[14] The reaction mixture was evaporated, and the residue was dissolved in a mixed solvent of toluene and *n*-hexane (1 : 3 in volume) and subjected to column chromatography. The reddish fraction was collected and condensed under reduced pressure to yield 3DBS$_4$-^{13}C (6 mg, 9%).

Unlabeled 3DBS$_2$ and 3DBS$_4$ were similarly prepared from double as much benzoyl chloride and pyridine as 1,3-propapedithiol in mole.

2.3 Synthesis of poly(alkylene dithioterephthalate) (PyTS$_2$)

Terephthaloyl chloride (20 mmol) was added under nitrogen atmosphere to α, ω-alkanedithiol (20 mmol) and triethyl amine (24 mmol) dissolved in a mixed solvent of cyclohexane (20 mL) and cyclohexanone (30 mL), and the solution was stirred at 60 °C for 6 h (y = 3) or 24 h (y = 4 and 5) to yield a white precipitate.[11] The white solid was collected by suction filtration, washed with water and methanol, dissolved in a mixed solvent of phenol and *o*-dichlobenzene, and poured into methanol to yield a precipitate, which was collected and dried under reduced pressure to yield PyTS$_2$: 43% (y = 3), 31% (y = 4), and 47% (y =5).

2.4 Synthesis of poly(alkylene tetrathioterephthalate) (PyTS$_4$)

PyTS$_4$ (y = 3 - 5) were synthesized by ionic polycondensation[12] between α, ω-dibromoalkane and tetrathioterephthalate acid complexed with piperidinium (S$_4$TPA-Pip)[14,15] dissolved in *N,N*-dimethylformamide (DMF) or dimethyl sulfoxide (DMSO).

As shown in Scheme 1, S$_4$TPA-Pip was prepared, and details of the handling were described previously.[12] S$_4$TPA-Pip was dissolved in DMF, and the solution was carefully degassed by the freeze-pump-thaw method with liquid nitrogen. α, ω-Dibromoalkane (exactly equimolar to S$_4$TPA-Pip) was dissolved in DMF, subjected to nitrogen purge and degasification, and added dropwise to the DMF solution of S$_4$TPA-Pip, and then the mixture was stirred at 50 °C for 45 h (y = 3), 60 h (y = 4), or 66 h (y = 5) to separate out red solid, which was collected by filtration, washed with DMF, water, and methanol, and dried under reduced pressure at 50 °C for 3 h to yield PyTS$_4$: 74% (y = 3); 77% (y = 4); 80% (y = 5).

Only for P3TS$_4$ and P4TS$_4$, the polymerization was conducted with DMSO as the solvent under the same conditions (temperature and reaction time); however, the yields were lower: 46% (y = 3); 32% (y = 4).

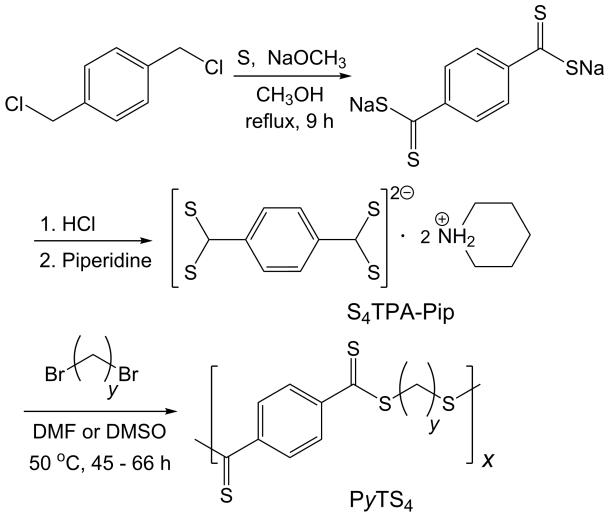

Scheme 1. Synthesis of PyTS$_4$ via S$_4$TPA-Pip.

2.5 Solution NMR

^{1}H (^{13}C) NMR spectra were recorded at 500 MHz (125.7 MHz) on a JEOL JNM-ECA500 spectrometer equipped with a variable temperature controller in the Center for Analytical Instrumentation of Chiba University. The sample temperatures were 15, 25, 35, 45, and 55 °C and maintained within ±0.1 °C fluctuations. Free induction decays were accumulated 64 (256) times. The pulse duration, data acquisition time, and recycle delay were 5.6 (5.0) μs, 3.3 (2.0) s, and 2.0 (2.0) s, respectively. In the ^{13}C NMR experiments, the gated decoupling technique was employed under the conditions given in the above parentheses. The solvents were cyclohexane-d_{12}, benzene-d_6, and dimethyl-d_6 sulfoxide, and the solute concentration was about 5 vol%. The observed NMR spectra were simulated with the gNMR program[16] to determine chemical shifts and coupling constants.

2.6 Solid state NMR

High-resolution ^{13}C cross polarization (CP) and pulse saturation transfer (PST) NMR experiments with magic angle spinning (MAS), abbreviated as CP/MAS and PST/MAS respectively, were carried out at a resonance frequency of 150.9 MHz on a JEOL JNM-ECA 600 spectrometer. The sample was packed in a silicon nitride rotor of 4 mm in diameter. The other conditions for the CP/MAS (PST/MAS) measurements were adjusted to each sample as follows: ^{1}H decoupler pulse duration, 3.5 μs (^{13}C pulse duration, 3.5 μs); contact time, 3.0 or 4.0 ms; relaxation delay, 2.5 – 7.0 (3.0) s; accumulation, 1000 – 12000 (1000 – 10000) times; spinning rate, 10.0 – 18.5 (10.0 – 18.5) kHz, where the parenthetic data are the PST/MAS parameters. The T_1 values were measured with Torchia's pulse sequence[17] of ^{13}C pulse duration = 3.5 μs under the same conditions as in the CP/MAS experiment.

2.7 Elemental analysis

Elemental analysis of S_4TPA-Pip was carried out by Systems Engineering Co. Ltd. with an Exeter Analytical CE440 Elemental Analyzer. The combustion and reduction temperatures were, respectively, 980 and 620 °C for carbon, hydrogen and nitrogen (CHN) analysis or 1080 and 850 °C for carbon, nitrogen, and sulfur (CNS) analysis, and the combustion time was 60 s. The standard and sample container were, respectively, acetanilide (sulphanilamide) and a tin capsule (a silver capsule) for the CHN (CNS) analysis.

Chlorine and bromine contents of S_4TPA-Pip were also determined by Nanotechno Service Co. Ltd. with a TOA DKK ICA-2000 ion chromatograph combined with a Yanaco New Science SQ-1 combustion furnace and HSU-35 absorption unit. The sample was combusted at 400 - 900 °C for 10 min and then at 1000 °C for 5 min, absorbed into aqueous dilute H_2O_2 or hydrazine solution, and subjected to ion chromatography under the following conditions: column, a Shodex IC SI-90 4E at 40 °C; eluent, 3.0 mM Na_2CO_3/2.0 mM $NaHCO_3$; flow rate, 1.2 mL min^{-1}; injection volume, 50 μL; detection, electrical conductivity detector.

2.8 Solubility test

Solubilities of P*y*TS$_2$ and P*y*TS$_4$ were investigated for a number of solvents. Powdered polymer (20 mg) and a given solvent (10 mL) were mixed, stirred at room temperature for 30 m, heated up to a temperature close to the boiling point of the solvent for 1 h, cooled down to room temperature, and stirred for 24 h, and then the mixture was observed to judge the degree of solubility visually.

2.9 Wide-angle X-ray diffraction

X-ray diffraction measurements were carried out by $\theta - 2\theta$ scans on a Bruker D8 Advance powder diffractometer. The incident X-ray beam was produced at 40 kV and 40 mA. The powdered specimen was put on a glass sample holder. The diffracted X-rays were detected by a scintillation counter.

2.10 Thermogravimetry (TG) and differential scanning calorimetry (DSC)

Thermogravimetric measurements were carried out with a Rigaku Thermo plus EVO II TG8120 under nitrogen atmosphere at a heating rate of 5 °C min^{-1}. DSC curves were recorded with a MAC DSC-3100 under nitrogen gas flow on first heating, first cooling, and second heating runs at a rate of 10 °C min^{-1}.

2.11 MO calculations

Density functional theoretical (DFT) and *ab initio* MO calculations were carried out with the Gaussian09 program[18] installed on an HPC Silent-SCC T2 or an HPC SCC System-L computer. For each conformer of 3DBS$_2$ or 3DBS$_4$, the geometry was fully optimized at the B3LYP/6-311+G(2d,p) level, and the thermal-correction term to the Gibbs free energy (at 25 °C) was also calculated. All self-consistent field (SCF) calculations were conducted under the tight convergence. With the optimized geometry, the electronic energy was computed at the MP2/6-311+G(2d,p) level. The Gibbs free energy was evaluated from the electronic and thermal-correction energies, being given here as the difference from that of the all-trans conformer and represented by ΔG_k (k: conformer). The ΔG_k values for the benzene medium at 25 °C were also calculated at the MP2/6-311+G(2d,p) level with the integral equation formalism of the polarizable continuum model (IEF-PCM).[19]

^{1}H and ^{13}C NMR chemical shifts[20] and ^{1}H–^{1}H and ^{13}C–^{1}H coupling constants[21] of $3DBS_2$ and $3DBS_4$ were calculated at the B3LYP/6-311++G(3df,3pd)//B3LYP/6-311+G(3df,3pd) level. ^{1}H and ^{13}C NMR chemical shifts of the S_4TPA-Pip complex and its subunits were evaluated at the B3LYP/6-311+G(3df,3pd)//B3LYP/6-311+G(2d,p) level.

Herein, the dihedral angle is defined according to the tradition in polymer science:[22] trans (t) ~ ±0°, cis (c) ~ ±180°, and gauche$^{\pm}$ (g$^{\pm}$) ~ ±120°. The dihedral angle (ϕ) can be converted to that (Φ) recommended by International Union of Pure and Applied Chemistry[23] according to $\Phi = -\mathrm{sign}(\phi)(180 - |\phi|)$, where the function, sign(ϕ), returns the sign of ϕ, and *vice versa*: $\phi = -\mathrm{sign}(\Phi)(180 - |\Phi|)$. Non-SI units are used: free energy in kcal mol^{-1} (1 kcal mol^{-1} = 4.184 kJ mol^{-1}); bond length in Å (1 Å= 10^{-10} m).

3 Results and discussion

3.1 NMR of $3DBS_2$ and $3DBS_4$

The polymer physicochemical doctrine that has been established by Flory *et al.*[22] shows that conformation- and configuration-dependent properties of a polymer in the Θ state (without the excluded volume effect) depend only on short-range intramolecular interactions, which can be predicted both theoretically and experimentally from small model compound(s) with the same bond sequence as the polymer includes. To elucidate conformational characteristics of the polymers treated here, therefore, it is significant to carry out conformational analysis of their small model compounds.

Herein, we first report conformational analysis of model compounds of $P3TS_2$ (Fig. 2a) and $P3TS_4$ (Fig. 2b) to discuss conformational characteristics of *S,S'*-(alkane-1,*y*-diyl) dibenzothioate (*y*DBS_2) and alkane-1,*y*-diyl dibenzodithioate (*y*DBS_4), *i.e.*, model compounds of P*y*TS_2 and P*y*TS_4 (*y* = 2 – 5) respectively.

Figs. 3 and 4, respectively, show NMR spectra observed from $3DBS_2$ (Fig. 2a) and $3DBS_4$ (Fig. 2b), model compounds of $P3TS_2$ and $P3TS_4$. To acquire quality ^{13}C NMR spectra, we synthesized $3DBS_2$-^{13}C and $3DBS_4$-^{13}C, one of whose carbonyl carbon was selectively labeled by ^{13}C. ^{1}H and ^{13}C NMR spectra of these ^{13}C-enriched models are also shown in Figs. 3 and 4. The gNMR simulation yielded chemical shifts and spin-spin coupling constants that satisfactorily reproduced both ^{1}H and ^{13}C NMR spectra measured under the same conditions (solvent and temperature). Of the data thus obtained, only vicinal coupling constants ($^{3}J_{CH}$, $^{3}J_{HH}$, and $^{3}J'_{HH}$) used in the conformational analysis are listed in Table 1, which shows the coupling constants of the models dissolved in cyclohexane-d_{12} at 15 – 55 °C, benzene-d_6 at 25 °C, and DMSO-d_6 at 25 °C.

From Newman projections in Fig. 5, the observed vicinal

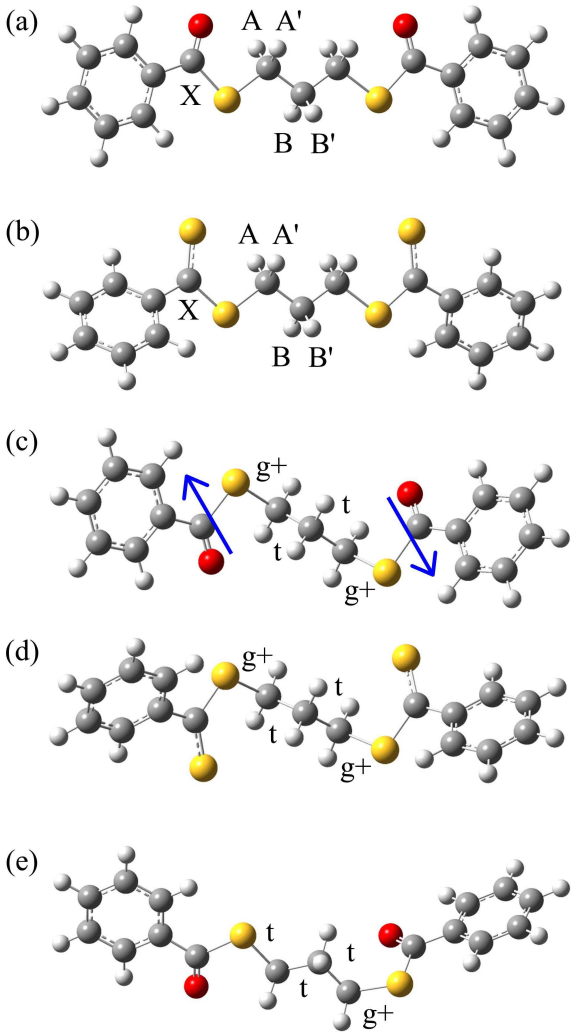

Fig. 2 Model compounds of poly(trimethylene dithioterephthalate) ($P3TS_2$) and poly(trimethylene tetrathioterephthalate) ($P3TS_4$): (a) *S,S'*-(propane-1,3-diyl) dibenzothioate-^{13}C ($3DBS_2$-^{13}C) in the all-trans (tttt) conformation; (b) propane-1,3-diyl dibenzodithioate-^{13}C ($3DBS_4$-^{13}C) in tttt; (c) $3DBS_2$ in g^{+}ttg^{+}; (d) $3DBS_4$ in g^{+}ttg^{+}; (e) $3DBS_2$ in tttg^{+}. The ^{13}C-labeled compounds in (a) and (b) were prepared for NMR experiments. The most stable conformations of $3DBS_2$ and $3DBS_4$ were predicted by MO calculations to be g^{+}ttg^{+}, and the crystal conformation of $3DBS_2$ is tttg^{+}.[13] The hydrogen and carbon atoms are partly alphabetized to represent the NMR spin system, and the arrow in (c) expresses the dipole moment at the thioester group.

coupling constants can be related to trans and gauche fractions of each bond:

$$^{3}J_{CH} = J_G p_t + \frac{J'_T + J'_G}{2} p_g \quad (1)$$

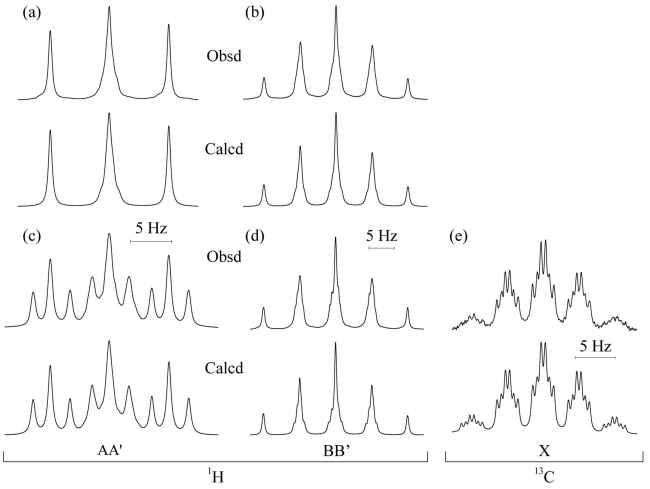

Fig. 3 Observed (above) and calculated (below) NMR spectra of (a-b) $3DBS_2$ and (c-e) $3DBS_2$-^{13}C dissolved in benzene-d_6 at 25 °C. For the nomenclature of hydrogen (A, A', B, and B') and carbon (X) atoms, see Fig. 2.

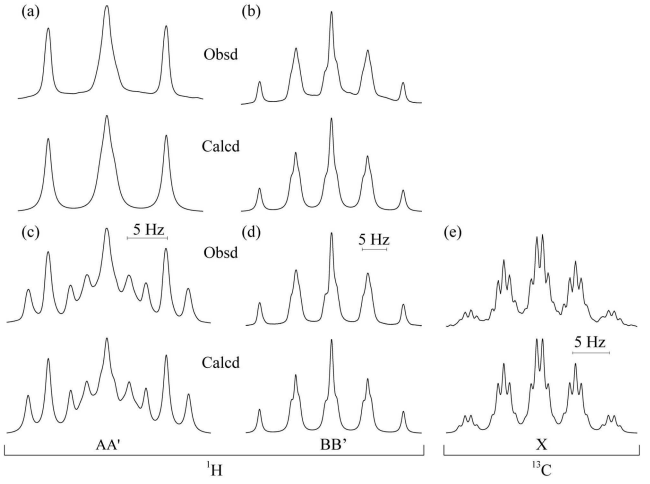

Fig. 4 Observed (above) and calculated (below) NMR spectra of (a-b) $3DBS_4$ and (c-e) $3DBS_4$-^{13}C dissolved in benzene-d_6 at 25 °C. For the nomenclature of hydrogen (A, A', B, and B') and carbon (X) atoms, see Fig. 2.

$$^3J_{HH} = {}^3J_{AB} = {}^3J_{A'B'} = J_G p_t + \frac{J'_T + J''_G}{2} p_g \quad (2)$$

and

$$^3J'_{HH} = {}^3J_{A'B} = {}^3J_{AB'} = J_T p_t + \frac{J'_G + J'''_G}{2} p_g \quad (3)$$

where J_T's and J_G's are illustrated in Fig. 5, and p_t and p_G are, respectively, trans and gauche fractions. By definition,

$$p_t + p_g = 1 \quad (4)$$

The coefficients, J_T's and J_G', were calculated from MO calculations for $3DBS_2$ and $3DBS_4$ at the B3LYP/6-311++G(3df,3pd) level or taken from the experimental values of 2-*tert*-butyl-1,3-dithiane including $-S-CH_2-CH_2-$ bond sequences.[24] The numerical data are given in the footnote of Table 1. From eqs. 1 and 4, the p_t and p_G values of the $S-CH_2$ bond were determined, while those of the CH_2-CH_2 bond were derived from eqs. 2 and 3 and divided by the sum of p_t and p_G thus obtained to satisfy eq. 4. On account of eq. 4, only the p_t values are listed in Table 1. If one notes that $p_{g^+} = p_{g^-} = p_g/2$, one can understand that the $S-CH_2$ and CH_2-CH_2 bonds have gauche and trans preferences, respectively.

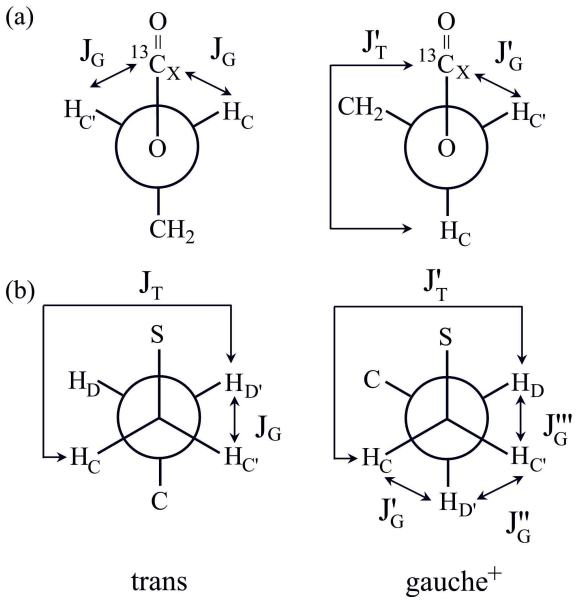

Fig. 5 Newman projections around the (a) $S-CH_2$ and (d) CH_2-CH_2 bonds, illustrating the coefficients, J_T's and J_G's, used in eqs. 1–3.

3.2 MO calculations on $3DBS_2$ and $3DBS_4$

Under the rotational isomeric state (RIS) approximation, the number of possible conformations of $3DBS_2$ and $3DBS_4$ may be 3^4 (= 81); however, the molecular symmetry leaves us with 25 irreducible conformations, which underwent the MO calculations at the MP2/6-311+G(2d,p)//B3LYP/6-311+G(2d,p) level to yield the Gibbs free energies as shown in Table 2. In common with $3DBS_2$ (Fig. 2c) and $3DBS_4$ (Fig. 2d), the lowest-energy conformer is g^+ttg^+, which seems to be stabilized by an intramolecular dipole-dipole interaction. However, we can find a number of conformers with free energies close to that of g^+ttg^+. The trans fractions of the $S-CH_2$ and CH_2-CH_2 bonds, calculated from the ΔG_k (k, conformer number) values, are compared in Table 1 with those determined by

Table 1 Vicinal coupling constants and trans fractions (p_t's) of $3DBS_2$ and $3DBS_4$

Medium	Temp (°C)	$^3J_{HH}$ [b]	$^3J'_{HH}$ [b]	$^3J_{CH}$ [b]	p_t CH_2-CH_2 set A [c]	p_t CH_2-CH_2 set B [d]	p_t $S-CH_2$ [a]
		$3DBS_2$ (NMR expt)					
Cyclohexane-d_{12}	15	6.61	7.50	4.55	0.42	0.44	0.14
	25	6.62	7.47	4.53	0.42	0.44	0.15
	35	6.66	7.47	4.52	0.42	0.43	0.15
	45	6.66	7.47	4.46	0.42	0.43	0.16
	55	6.72	7.46	4.46	0.41	0.43	0.16
Benzene-d_6	25	6.47	7.84	4.46	0.45	0.47	0.16
Dimethyl-d_6 sulfoxide	25	6.40	7.94	4.48	0.47	0.48	0.16
		$3DBS_2$ (MO calc)					
Gas	15				0.44		0.11
	25				0.44		0.12
	35				0.44		0.12
	45				0.43		0.12
	55				0.43		0.12
Benzene	25				0.46		0.14
		$3DBS_4$ (NMR expt)					
Cyclohexane-d_{12}	15	6.48	7.89	5.40	0.47	0.47	0.20
	25	6.50	7.89	5.37	0.46	0.47	0.20
	35	6.50	7.88	5.34	0.46	0.47	0.21
	45	6.54	7.84	5.30	0.46	0.46	0.21
	55	6.54	7.83	5.27	0.46	0.46	0.22
Benzene-d_6	25	6.43	8.14	5.25	0.48	0.49	0.22
Dimethyl-d_6 sulfoxide	25	6.35	8.11	5.35	0.49	0.49	0.20
		$3DBS_4$ (MO calc)					
Gas	15				0.38		0.19
	25				0.38		0.19
	35				0.38		0.20
	45				0.38		0.20
	55				0.38		0.21
Benzene	25				0.41		0.22

[a] From MO calculations: J_G = 1.08, J'_T = 6.39, and J'_G = 3.86 Hz for $3DBS_2$; J_G = 1.14, J'_T = 8.17, and J'_G = 4.69 Hz for $3DBS_4$ (this study).

[b] In Hz.

[c] From MO calculations: J_T = 12.55, J_G = 3.81, J'_T = 11.58, J'_G = 2.40, J''_G = 3.59, and J'''_G = 2.79 Hz for $3DBS_2$; J_T = 12.58, J_G = 3.77, J'_T = 11.76, J'_G = 2.39, J''_G = 3.81, and J'''_G = 2.70 Hz for $3DBS_4$ (this study).

[d] From experimental J_T and J_G values of 2-*tert*-butyl-1,3-dithiane.[24]

the NMR experiments. In general, the agreement between theory and experiment is satisfactory.

3.3 Odd-even effects of model compounds

Our previous study[12] dealt with *S,S'*-(ethane-1,2-diyl) dibenzothioate ($2DBS_2$) and ethane-1,2-diyl dibenzodithioate ($2DBS_4$). These models also show gauche and trans preferences in the $S-CH_2$ and CH_2-CH_2 bonds respectively, being most stabilized in the g^+tg^- (termed often 'kink') conformation, which renders the two phenyl rings parallel and forms an intramolecular dipole-dipole attraction.[26,27] Because the difference in electronegativity between carbon and oxygen is larger than that between carbon and sulfur, the −S−C=O group is superior to −S−C=S in dipole moment. Accordingly, the g^+tg^- conformer of $2DBS_2$ has a ΔG_k value of −3.13 kcal mol^{-1}, while that of $2DBS_4$ was evaluated to be −2.08 kcal mol^{-1}. As mentioned above, $3DBS_2$ and $3DBS_4$ also form the dipole-dipole interactions in the g^+ttg^+ state. However, $3DBS_2$ crystallizes in $tttg^+$,[13] while $3DBS_4$ remains liquid at room temperature. The crystalline $4DBS_2$ and $5DBS_2$ adopt g^+tttg^- and $tttttg^+$ conformations, respectively.[13,28] The former is analogous to the kink conformation of $2DBS_2$, and the latter to $tttg^+$ of $3DBS_2$. The crystal conformation of $4DBS_4$ is tg^+tg^-t including the kink trio at the center.[29]

The melting point (T_m) may represent the crystal stability: 94 °C ($2DBS_2$); 59 °C ($3DBS_2$); 49 °C ($4DBS_2$); 49 °C ($5DBS_2$); 109 °C ($2DBS_4$); −51 °C ($3DBS_4$); 68 °C ($4DBS_4$); −53 °C ($5DBS_4$). The thioesters weakly show the odd-even oscillation in T_m, whereas the dithioesters do show strongly. In our previous study,[30] the similar odd-even effect was clearly observed in crystal and mesophase stabilities of model compounds of liquid crystalline polyethers.

Table 2 Conformer free energies of $3DBS_2$ and $3DBS_4$, evaluated from MO calculations

					$\Delta G_k{}^a$ (kcal mol^{-1})			
					$3DBS_2$		$3DBS_4$	
k	Conformation^b				Gas	C_6H_6	Gas	C_6H_6
1	t	t	t	t	0.00	0.00	0.00	0.00
2	t	t	t	g^+	−1.23	−1.09	−0.77	−0.66
3	t	t	g^+	t			−0.02	0.07
4	t	t	g^+	g^+	−0.84	−0.70	−0.85	−0.65
5	t	t	g^+	g^-	−0.60	−0.33	−0.38	−0.27
6	t	g^+	t	g^+	−0.49	−0.33	−1.14	−1.01
7	t	g^+	t	g^-	−1.63	−1.39	−1.30	−1.12
8	t	g^+	g^+	t	−0.55	−0.50	−0.28	−0.10
9	t	g^+	g^+	g^+	−2.09	−1.82	−1.12	−0.79
10	t	g^+	g^+	g^-			−0.56	−0.44
11	t	g^+	g^-	t			0.05	0.23
12	t	g^+	g^-	g^+			−1.50	−1.22
13	t	g^+	g^-	g^-	1.72	1.94	−0.72	−0.53
14	g^+	t	t	g^+	−2.71	−2.40	−2.10	−1.83
15	g^+	t	t	g^-	−0.91	−0.69		
16	g^+	t	g^+	g^+	−2.25	−1.94	−1.78	−1.55
17	g^+	t	g^+	g^-			−1.21	−0.84
18	g^+	t	g^-	g^+	−2.23	−1.82	−1.13	−0.83
19	g^+	t	g^-	g^-	−2.13	−1.76	−1.41	−1.10
20	g^+	g^+	g^+	g^+	−2.52	−2.03	−1.74	−1.26
21	g^+	g^+	g^+	g^-	−1.85	−1.43	−1.54	−1.16
22	g^+	g^+	g^-	g^+	−0.70	−0.31		
23	g^+	g^+	g^-	g^-	−0.13	0.25	−1.50	−1.13
24	g^+	g^-	g^+	g^-				
25	g^+	g^-	g^-	g^+				

^{a}At the MP2/6-311+G(2d,p)//B3LYP/6-311+G(2d,p) level. ^{b}Of the spacer: S−CH_2−CH_2−CH_2−S bonds. The blank represents that the local minimum of the potential was not found by the geometrical optimization.

3.4 Complex monomer of P*y*TS_4, S_4TPA-Pip

In the previous study,[12] we found a novel polymerization method for $P2TS_4$: ionic polycondensation of S_4TPA-Pip and 1,2-dibromoethane. Then, the ratio of tetrathioterephthalate acid (S_4TPA) to piperidinium (Pip) was determined to be 1:4 from integrated intensities of its ^{1}H NMR; however, the chemical structure of minus-quadrivalent tetrathioterephthalate could not be depicted according to the conventional valence-bond concept. To establish the polymerization method, therefore, we have revisited the structural determination of the S_4TPA-Pip complex. Fig. 6 shows a ^{1}H NMR spectrum of S_4TPA-Pip in DMSO at room temperature. In the experimental spectrum, the relative intensities and assignment are indicated. In the region of 7.0 − 8.2 ppm, a number of small peaks appear around the intense signal at 7.9 ppm of the aromatic protons. Only from the intense peak, the S_4TPA to Pip ratio can be estimated to be 1:4 as before. If the small signals are also included, the integrated intensity doubly increase to be 4.0 as written in the spectrum, and hence the S_4TPA to Pip ratio may possibly be modified to 1:2.

Furthermore, S_4TPA-Pip underwent elemental analysis, and the results are shown in Table 3. The composition as obtained is given on the line of 'As measured', and the total percentage of the five elements was 95.74%. Accordingly, all the elemental compositions were multiplied by a factor of 100/95.74 to be modified to the 'Normalized' data. The calibrated values are in good agreement with the 'Calculated' data that were evaluated from S_4TPA : Pip = 1:2, because the experimental tolerances were estimated as 0.3% for C, H, and N and 0.6% for S and Cl. As shown above, it seems acceptable that one S_4TPA anion forms a complex with exactly two Pip cations. The oxygen and water dissolved in the NMR solvent, DMSO, might degrade S_4TPA, or the complex structure in the solution would not be uniform, and hence the aromatic protons undergo different chemical shieldings to generate the small signals, although the solidified S_4TPA-Pip appears to be stable even in the air.

^{1}H and ^{13}C NMR chemical shifts of dianionic and minus-quadrivalent S_4TPA's dissolved in DMSO were calculated by the gauge-independent atomic orbital (GIAO) method[20] at the B3LYP/6-311+G(3df,3pd) level with the solvation effect of the IEF-PCM model.[19] The ^{1}H and ^{13}C NMR chemical shifts (in δ ppm) relative to that (0 ppm) of tetramethyl silane (TMS) are plotted in Figs. 6 and 7 respectively and compared with ex-

Table 3 Elemental analysis of S_4TPA-Pip

	Elemental composition (%)					
	C	H	N	S	Cl	Total
Calcd	53.96	7.04	6.99	32.01	0.00	100.00
As measured	51.84	6.68	6.50	30.55	0.17	95.74
Normalized [a]	54.15	6.98	6.79	31.91	0.18	100.01

[a] The 'As measured' compositions were multiplied by a factor of 100/95.74 to yield the 'Normalized' data.

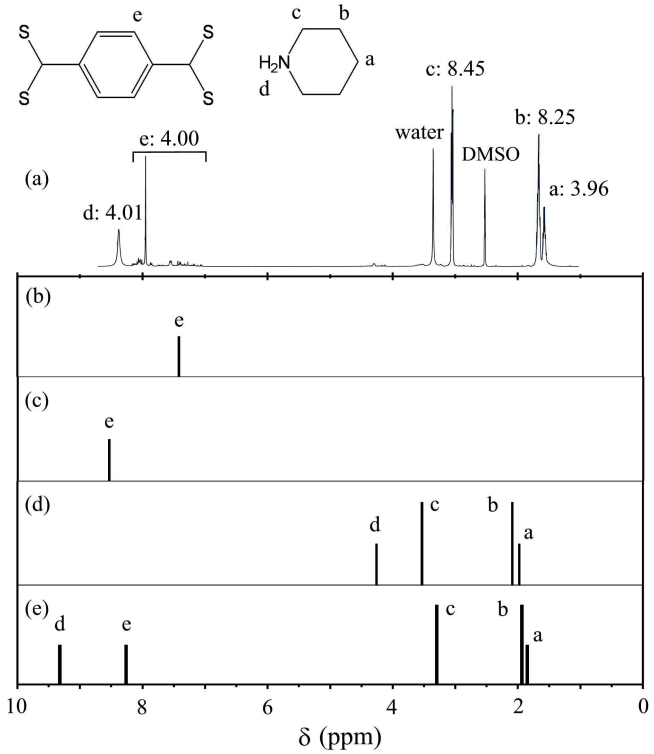

Fig. 6 (a) Observed and (b – e) calculated ^{1}H NMR spectra of (a, e) the complex (abbreviated as S_4TPA-Pip) of tetrathioterephthalate acid (S_4TPA) with piperidinium (Pip), (b) S_4TPA^{4-}, (c) S_4TPA^{2-}, and (d) Pip. The peaks were assigned as shown, and the numerical values in (a) represent the integrated intensities.

periment. The chemical shifts of TMS were also calculated at the same level. In the experimental ^{1}H NMR spectrum, proton e appears at 7.9 ppm (Fig. 6a) close to the mean value of the calculated δ's of S_4TPA^{4-} (7.42 ppm, Fig. 6b) and S_4TPA^{2-} (8.54 ppm, Fig. 6c). The S−C−S carbon (designated as carbon G) of S_4TPA^{4-} shows a peak at 175 ppm, whereas δ_C of S_4TPA^{2-} is 281 ppm, relatively close to the experimental value (251 ppm). The calculated ^{1}H and ^{13}C NMR spectra of Pip are plotted in Figs. 6d and 7d, respectively. The superposition ^{13}C NMR spectra of S_4TPA^{2-} (Fig. 7c) and $2Pip^+$ (Fig. 7d) is close to the observation, whereas this is not case with the ^{1}H NMR; proton d (NH_2) is observed at a much lower magnetic field (8.3 ppm).

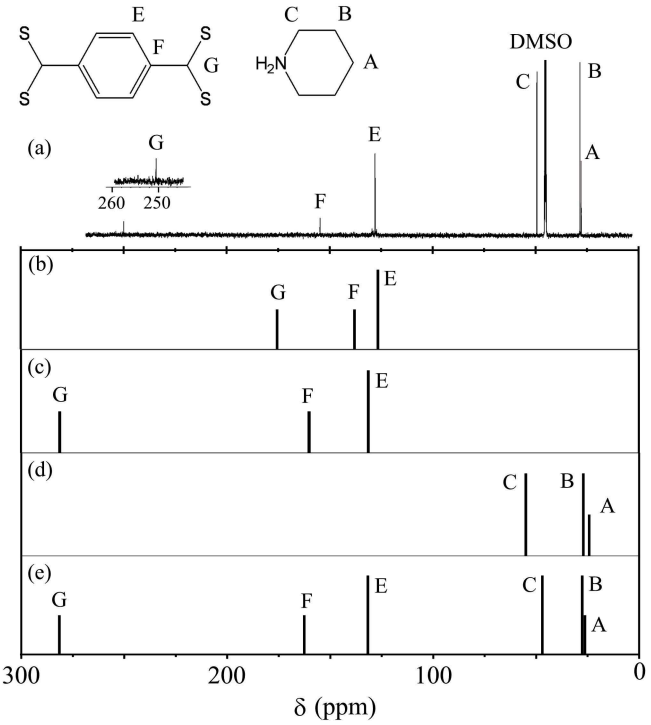

Fig. 7 (a) Observed and (b – e) calculated broadband proton decoupled ^{13}C NMR spectra of (a, e) S_4TPA-Pip, (b) S_4TPA^{4-}, (c) S_4TPA^{2-}, and (d) Pip. The peaks were assigned as shown.

Accordingly, we attempted to calculate the chemical shifts of the S_4TPA-Pip_2 complex. The S_4TPA^{2-} and two Pip^+ molecules were initially set as optimized individually, and the N−N−H and S−C−S groups were so arranged as to face each other. The geometrical optimization and chemical-shift calculation for the S_4TPA-Pip_2 complex in DMSO were carried out. Fig S1 (Supplementary Information) shows the optimized structure, and Figs. 6e and 7e schematically illustrate the calculated NMR spectra. The ^{13}C NMR spectrum is similar to

the superposition, whereas the ^{1}H NMR exhibits proton d at 9.3 ppm, thus being in fairly good agreement with the experiment. The sulfur atoms of S_4TPA probably produce a strong electron-withdrawing effect on the NH_2 protons of Pip. From the above discussion, we can conclude that S_4TPA forms a complex with two Pip molecules.

3.5 Synthesis of P*y*TS$_2$ and P*y*TS$_4$

The polythioesters P*y*TS$_2$ were prepared from terephthaloyl chloride and α, ω-alkanedithiol (HS−(CH$_2$)$_y$−SH). The polydithioesters P*y*TS$_4$ were synthesized by the ionic polycondensation between S_4TPA-Pip and α, ω-dibromoalkane in DMF at 50 °C; the polymerization time and yield were 45 h and 74% (y = 3), 60 h and 77% (y = 4), and 66 h and 80% (y = 5). The yields are high. As will described later, P3TS$_4$ and P4TS$_4$ exhibit a singular thermal transition. To investigate whether its occurrence and temperature depend on the polymerization solvent, the two polydithioesters were also synthesized in DMSO at 50 °C; the reaction times were set equal to those for DMF, but the yields were lower: 46% (y = 3) and 32% (y = 4). The thermal transition appeared at almost the same temperature irrespective of the used solvent.

Solid state ^{13}C CP/MAS NMR spectra observed from the synthesized polythioesters and polydithioesters are shown in Figs. S2 and S3, respectively, (Supplementary Information); all the signals could be assigned to the constituent carbon atoms.

3.6 Solubility of P*y*TS$_2$ and P*y*TS$_4$

Solubilities of P*y*TS$_2$ and P*y*TS$_4$ were investigated for a number of solvents. Both P*y*TS$_2$ and P*y*TS$_4$ are insoluble in ordinary organic solvents such as toluene, *n*-hexane, chloroform, dichloromethane (DCM), acetone, DMF, and DMSO, but soluble in some acidic solvents used often for aromatic polyesters, *e.g.*, trifluoroacetic acid (TFA), hexafluoroisopropanol (HFIP), phenol, and mixed solvents of TFA and DCM (1:3 in volume), HFIP and DCM (1:3), and *o*-dichlorobenzene and phenol (3:2) as shown in Table 4. In general, the solubility of P*y*TS$_2$ tends to be improved with an increase in y, whereas P*y*TS$_4$ show no clear tendency.

Inasmuch as both kinds of polymers are soluble only in the organic acids, the molecular weights could not be directly measured by *e.g.*, static light scattering. This is because such acidic solvents are usually prohibited to be used in differential refractometers. The matrix-assisted laser desorption/ionization time-of-flight mass (MALDI-TOF-MS) experiments were also attempted, but in vain.

Poly(ethylene dithioterephthalate) (P2TS$_2$) was prepared according to the German patent,[11] in which its degree of polymerization was estimated to be larger than 40. Therefore, the polythioesters prepared here may have the comparable molecular weights. To our knowledge, however, we first synthesized PyTS$_4$. The monomers and, probably, the small oligomers are soluble in common organic solvents; therefore, the insolubility of PyTS$_4$ suggests the polymer formation. This is because the polymer thermodynamics[25,31] shows that the solubility of a polymer tends to be reduced with increasing molecular weight: volume fractions of a polymer in precipitated and supernatant phases, v'_x and v_x respectively, are related by $v'_x/v_x = \exp(\alpha x)$, where α is the partition factor, and x is the number of segments and hence proportional to the molecular weight.

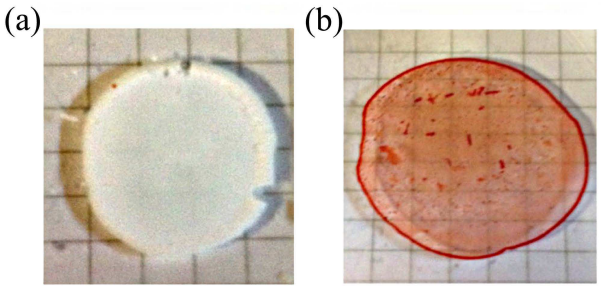

Fig. 8 Films cast from phenol solutions of (a) P3TS$_2$ and (b) P3TS$_4$. Each film was cast in a small petri dish, peeled off, and placed on a 3-mm graph paper to be photographed.

As shown in Fig 8, we successfully cast films of P3TS$_2$ and P3TS$_4$ from the phenol solutions and, at least, proved that the polymers have enough molecular weights to form the films. The P3TS$_2$ film is opaque white, while the P3TS$_4$ film is red and transparent.

3.7 Thermal analysis

Table 5 summarizes the results of thermal analyses. All the PyTS$_2$'s except y = 2 melt over 200 °C, whereas all the PyTS$_4$'s exhibit no melting. Irrespective of y, PyTS$_2$ decomposed around 350 °C, and PyTS$_4$ in the range of 220 − 260 °C. The glass transition of PyTS$_2$ appears around room temperature, while T_g of P*y*TS$_4$ decreases from 71 to 26 °C with increasing y.

As shown in Fig. 9, P3TS$_4$ and P4TS$_4$ show a sharp endothermic peak at 143 and 134 °C, respectively. On the second heating, however, the endotherm was not observed; therefore, this phenomenon is irreversible. Inasmuch as no weight change occurred there, it is due to neither transpiration of the residual solvent nor partial thermal decomposition. The powder of P3TS$_4$ or P4TS$_4$ was put in a testing tube, which was degassed and sealed, and heated at 150 °C for 2 h. As a result, the sample changed its color to deep Indian red as shown in Fig. S6 (Supplementary Information). The samples were heated gradually up to 230 °C but did not exhibit any fluidity

Table 4 Solubilities of the aromatic polythioesters (P*y*TS$_2$) and polydithioesters (P*y*TS$_4$) [a]

	PyTS$_2$: *y*				PyTS$_4$: *y*			
Solvent [b]	2	3	4	5	2	3	4	5
TFA	—	—	—	+	—	—	—	—
HFIP	—	—	—	+	—	—	—	—
TFA/DCM (1:3)	—	—	+	+	±	±	—	—
HFIP/DCM (1:3)	—	—	±	+	±	±	—	—
Phenol	—	+	+	+	±	+	±	±
DCB/Phenol (3:2)	—	+	±	+	±	+	±	±
conc. H_2SO_4 [c]	—	+	+	+	×	×	×	×

[a] Symbols: +, soluble; ±, slightly soluble; —, insoluble; ×, degraded.

[b] Abbreviations: TFA, trifluoroacetic acid; HFIP, hexafluoroisopropanol; DCM, dichloromethane; DCB, *o*-dichlorobenzene.

[c] Heated up to 100 °C.

even after the color change; therefore, the endothermic change does not correspond to melting.

3.8 X-ray diffraction

Fig. 10 shows powder X-ray diffraction patters observed from as-precipitated (*i.e.*, unannealed) samples of P*y*TS$_2$ and P*y*TS$_4$ ($y = 2 - 5$). All the samples of P*y*TS$_2$ exhibit diffraction peaks, which indicate the existence of the crystalline phase. On the other hand, P3TS$_4$ and P4TS$_4$ are suggested to include crystallites, and P2TS$_4$ and P5TS$_4$ seem to be completely amorphous.

As discussed above, only P3TS$_4$ and P4TS$_4$ exhibit the endothermic change at 143 and 134 °C, respectively. Fig. 10 also includes X-ray diffraction diagrams of P3TS$_4$ and P4TS$_4$ annealed at 150 °C for 2 h; no diffraction peak was observed therefrom, and hence the endothermic change may be a crystalline-to-amorphous transition.

3.9 Solid state NMR

Fig. 11 shows solid state ^{13}C CP/MAS and PST/MAS NMR spectra of the as-precipitated and annealed P3TS$_4$ and P4TS$_4$ samples, and the observed peaks are assigned as indicated. It is known that the PST/MAS method emphasizes signals of high-mobility spins in the amorphous region.[32] Because the CP/MAS spectra of the annealed samples exactly agree with PST/MAS in peak position, these two spectra reflect the amorphous phase, and the differences in CP/MAS between the as-precipitated and annealed samples stem from the crystalline phase. Accordingly, the chemical shifts of carbons a, b, and d were assigned to the crystalline and amorphous phases as indicated in Fig. 11.

The longitudinal relaxation times, T_1's, of the as-precipitated and annealed P3TS$_4$ and P4TS$_4$ were measured with Torchia's pulse sequence.[17] The data are listed in Table 6. By the annealing at 150 °C for 2 h, the T_1 values of the methylene groups of P3TS$_4$ were reduced from 130 to a few seconds. The aromatic groups have larger T_1's than the methylene units, thus being more restricted in mobility. Without the annealing, P4TS$_4$ shows smaller T_1's and higher mobility than P3TS$_4$. It should be noted that T_g's of P3TS$_4$ and P4TS$_4$ are 44 and 27 °C, respectively; P4TS$_4$ is more active in molecular motion at ambient temperature. After the annealing, P4TS$_4$ has T_1's close to those of P3TS$_4$. These results also support the conclusion that the endothermic change corresponds to a crystalline-to-amorphous transition.

4 Summary

Herein, we have described (1) the *y* dependence of conformational characteristics of P*y*TS$_2$ and P*y*TS$_4$ ($y = 2 - 5$) via NMR and single crystal X-ray diffraction experiments and MO calculations on their model compounds, (2) the detailed investigation of the monomer, S$_4$TPA-Pip, adopted in the synthesis of P*y*TS$_4$, and (3) characterization of P*y*TS$_2$ and P*y*TS$_4$ by various experimental methods. The summary is as follows.

Both 2DBS$_2$ and 2DBS$_4$ are most stabilized in the g$^+$tg$^-$ state and crystallize in this conformation, which forms an intramolecular dipole-dipole interaction between the thioester (dithioester) groups. The most stable conformation of 3DBS$_2$ and 3DBS$_4$ is g$^+$ttg$^+$, which also forms the dipole-dipole interaction. The crystal conformation of 3DBS$_2$ is tttg, whereas 3DBS$_4$ does not crystallize at ambient temperature. 4DBS$_2$, 4DBS$_4$, and 5DBS$_2$ crystallize into g$^+$tttg$^-$, tg$^+$tg$^-$t, and tttttg$^+$ conformations, respectively. To sum up, the S–CH$_2$ and CH$_2$–CH$_2$ bonds possess the gauche and trans preferences respectively, and the intramolecular dipole-dipole interactions also influence the spacer conformation. The thioesters and dithioesters, respectively, depending on *y*, exhibit weak and

Table 5 Thermal properties of the aromatic polythioesters (P*y*TS$_2$) and polydithioesters (P*y*TS$_4$)

	P*y*TS$_2$: *y*				P*y*TS$_4$: *y*			
	2	3	4	5	2	3	4	5
T_g [a] (°C)	36	40	20	22	71	44	27	26
T_m [b] (°C)	— [c]	202	225	181, [d] 209	— [c]	(143,[e] 153[f])	(134, [e] 134 [f])	— [c]
ΔH [g] (kcal mol^{-1})		1.80	0.52	0.29, [d] 0.63		(1.64,[e] 1.79 [f])	(1.27, [e] 0.69 [f])	
T_d [h] (°C)	346	350	349	354	220	260	225	240

[a] The glass transition temperature observed by DSC. [b] The melting point observed by DSC. [c] Not detected. [d] Probably, a crystal-to-crystal transition prior to melting. [e] The crystalline-to-amorphous transition of the sample polymerized in DMF. [f] The crystalline-to-amorphous transition of the sample polymerized in DMSO. [g] The enthalpy change of the transition given just above on the line of T_m, as estimated from the DSC measurement. [h] The thermal degradation temperature was determined from the intersection of two tangents on the TG curve before and after the beginning of the weight loss.

Table 6 Chemical shifts (δ's) and longitudinal relaxation times (T_1's) of as-precipitated and annealed P3TS$_4$ and P4TS$_4$ samples

	P3TS$_4$				P4TS$_4$			
	As-precipitated		Annealed		As-precipitated		Annealed	
Peak	δ (ppm)	T_1 (s)	δ (ppm)	T_1 (s)	δ (ppm)	T_1 (s)	δ (ppm)	T_1 (s)
a	29.5	131.2	28.0	3.1	29.1	54.5	28.6	1.2
b	35.9	130.8	37.2	2.1	37.3	54.0	37.3	2.0
c	145.2	240.5	145.2	38.2	145.7	72.4	145.7	28.6
d_1 [a]	124.9	180.2			125.1	99.4		
d_2 [b]			128.0	16.8			127.7	16.4
d_3 [a]	128.9	139.5			129.2	52.4		
e [c]	224.9		224.9		224.6	112.1	224.6	

[a] From the crystalline phase in the as-precipitated sample.
[b] From the amorphous phase in the annealed sample.
[c] The blank represents that the T_1 value is too large to be determined under the experimental conditions.

strong odd-even oscillations in melting point.

^{1}H and ^{13}C NMR spectra observed from S$_4$TPA-Pip were simulated from DFT calculations and satisfactorily reproduced with a complex model of S$_4$TPA : Pip ratio = 1:2, and the stoichiometry was confirmed by elemental analysis. The ionic polycondensation using S$_4$TPA-Pip was proved to be applicable to PyTS$_4$'s (y = 3 - 5) as well as P2TS$_4$. Both P*y*TS$_2$ and P*y*TS$_4$ are insoluble in common organic solvents such as toluene, *n*-hexane, chloroform, DCM, acetone, DMF, and DMSO, but soluble in organic acids, *e.g.*, TFA, HFIP, and phenol. Films of P3TS$_2$ and P3TS$_4$ were successfully cast from the phenol solutions.

The glass transitions of PyTS$_2$ occur around room temperature, and T_g of PyTS$_4$ decreases with an increase in y: 71 °C (y = 2) to 26 °C (y = 5). P*y*TS$_2$ melt over 200 °C and decompose around 350 °C, whereas P*y*TS$_4$ show no melting until thermal degradation occurs (220 − 260 °C). However, P3TS$_4$ and P4TS$_4$ exhibit an endothermic change at 130 − 150 °C. At the endotherm the two polydithioesters change the color to deep Indian red but exhibit no fluidity up to the thermal decomposition. X-ray diffraction and solid state NMR experiments showed that the endothermic change is an irreversible crystalline-to-amorphous transition.

As compared with the aromatic polyesters such as PET, PTT, and PBT, both P*y*TS$_2$ and P*y*TS$_4$ are more difficult to dissolve in solvents, *i.e.*, superior in chemical resistance. In contrast, the thermal resistance may be evaluated to be in the order of P*y*TS$_4$ < P*y*TS$_2$ < polyesters. The polythioesters are semicrystalline, whereas the polydithioesters are, in general, amorphous, exhibit no melting, and have reddish colors. Owing to the advantages and in spite of the disadvantages, hopefully, the novel polymers will be put into practical use. As stated above, we have developed chemistry of the aromatic polythioesters and polydithioesters.

Acknowledgements

We thank Systems Engineering Co. Ltd. and Nanotechno Service Co. Ltd. for the elemental analysis. This study was

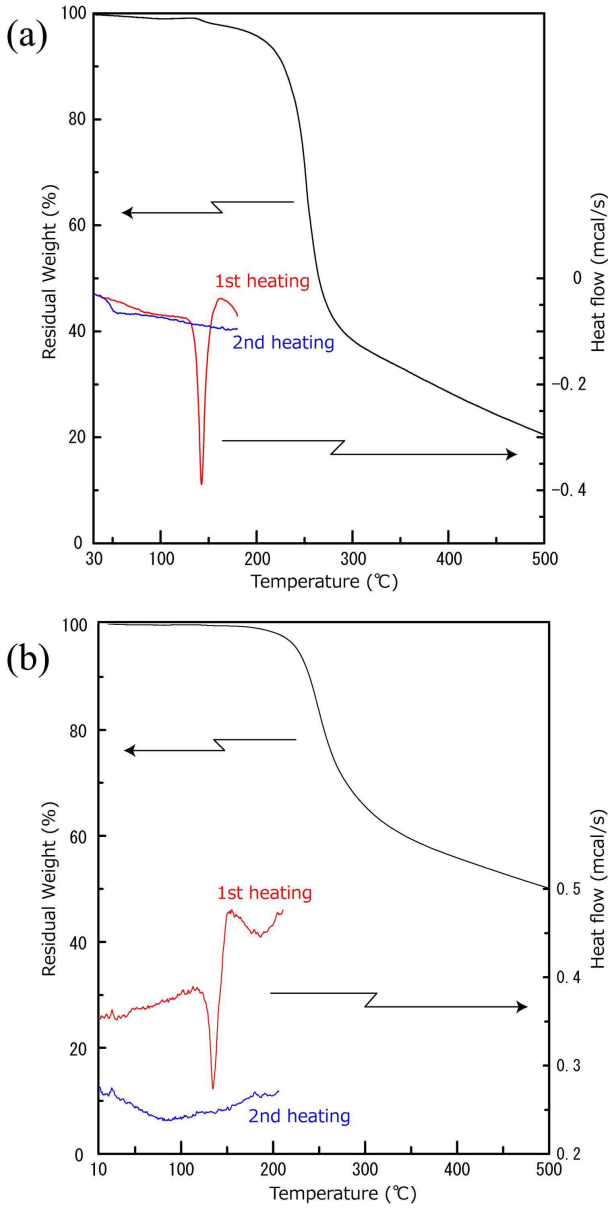

Fig. 9 Thermogravimetric (TG, left vertical axis) and differential scanning calorimetric (DSC, right vertical axis) charts of (a) $P3TS_4$ and (b) $P4TS_4$ polymerized in DMF.

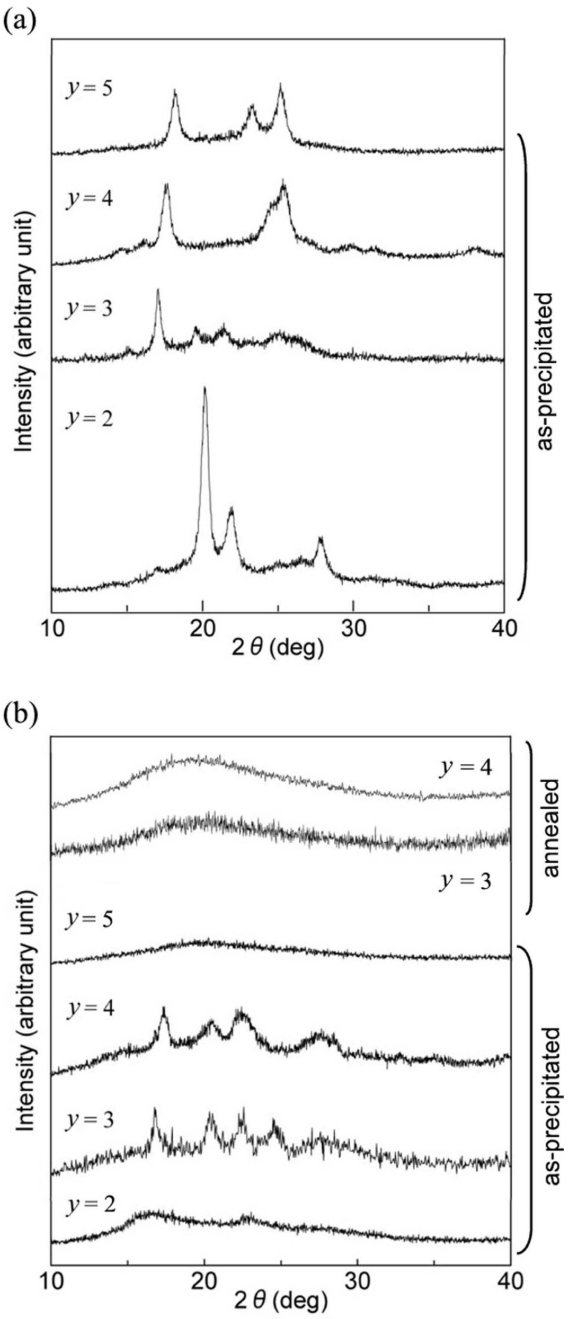

Fig. 10 Powder X-ray diffraction diagrams of (a) as-precipitated $PyTS_2$ and (b) as-precipitated and annealed $PyTS_4$, where y is the number of methylene groups in the spacer.

partly supported by a Grant-in-Aid for Scientific Research (C) (22550190) from the Japan Society for the Promotion of Science.

References

1 *Polymer Data Handbook*, ed. J. E. Mark, Oxford University Press, New York, USA, 1999.
2 K. Tashiro, *Prog. Polym. Sci.*, 1993, **18**, 377–435.
3 R. de P. Daubeny, C. W. Bunn and C. J. Brown, *Proc. Roy. Soc. A*, 1954, **226**, 531–542.
4 S. Poulin-Dandurand, S. Pérez, J.-F. Revol and F. Brisse, *Polymer*, 1979, **20**, 419–426.
5 I. J. Desborough, I. H. Hall and J. Z. Neisser, *Polymer*, 1979, **20**, 545–552.

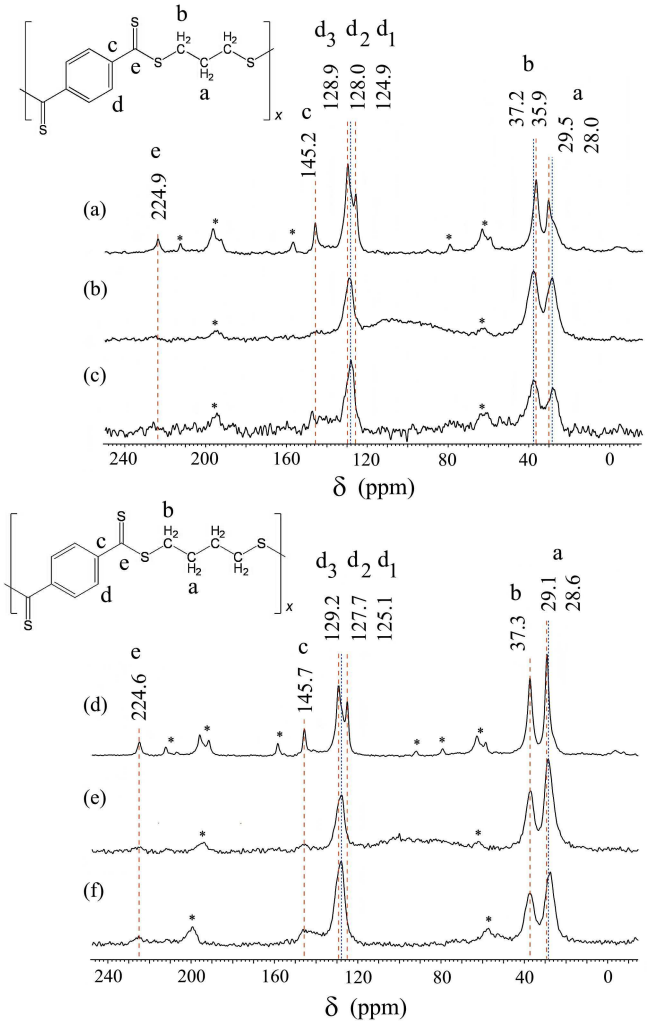

Fig. 11 Solid state ^{13}C NMR spectra of $P3TS_4$ and $P4TS_4$: $P3TS_4$, as-precipitated sample by (a) CP/MAS and (b) PST/MAS and (c) annealed sample by CP/MAS; $P4TS_4$, as-precipitated sample by (d) CP/MAS and (e) PST/MAS and (f) annealed sample by CP/MAS. The individual signals were assigned as shown, and the asterisks represent spinning side bands.

6 T. Nishino, T. Okamoto and H. Sakurai, *Macromolecules*, 2011, **44**, 2106–2111.
7 Z. Mencik, *J. Polym. Sci., Polym. Phys. Ed.*, 1975, **13**, 2173–2181.
8 M. Yokouchi, Y. Sakakibara, Y. Chatani, H. Tadokoro, T. Tanaka and K. Yoda, *Macromolecules*, 1976, **9**, 266–273.
9 Wingfoot Corporation, Linear polythioesters, British Patent 630,625, October 18, 1949.
10 C. S. Marvel and A. Kotch, *J. Am. Chem. Soc.*, 1951, **73**, 1100–1102.
11 E. Mack and H. R. Thönnessen, Thioester Polymer, German Patent 2,016,631, October 21, 1971.
12 D. Abe and Y. Sasanuma, *Polym. Chem.*, 2012, **3**, 1576–1587.
13 C. Leblanc and F. Brisse, *Can. J. Chem.*, 1992, **70**, 900–909.
14 M. P. Cava and M. I. Levinson, *Tetrahedron*, 1985, **41**, 5061–5087.
15 Y. Ueno, M. Bahry and M. Okawara, *Tetrahedron Lett.*, 1977, 4607–4610.
16 P. H. Budzelaar, *gNMR,* version 5.0, IvorySoft & Adept Scientific plc, Letchworth, U.K., 2004.
17 D. A. Torchia, *J. Magn. Reson.*, 1978, **30**, 613–616.
18 M. J. Frisch, G. W. Trucks, H. B. Schlegel, G. E. Scuseria, M. A. Robb, J. R. Cheeseman, G. Scalmani, V. Barone, B. Mennucci, G. A. Petersson, H. Nakatsuji, M. Caricato, X. Li, H. P. Hratchian, A. F. Izmaylov, J. Bloino, G. Zheng, J. L. Sonnenberg, M. Hada, M. Ehara, K. Toyota, R. Fukuda, J. Hasegawa, M. Ishida, T. Nakajima, Y. Honda, O. Kitao, H. Nakai, T. Vreven, J. A. Montgomery, Jr., J. E. Peralta, F. Ogliaro, M. Bearpark, J. J. Heyd, E. Brothers, K. N. Kudin, V. N. Staroverov, R. Kobayashi, J. Normand, K. Raghavachari, A. Rendell, J. C. Burant, S. S. Iyengar, J. Tomasi, M. Cossi, N. Rega, J. M. Millam, M. Klene, J. E. Knox, J. B. Cross, V. Bakken, C. Adamo, J. Jaramillo, R. Gomperts, R. E. Stratmann, O. Yazyev, A. J. Austin, R. Cammi, C. Pomelli, J. W. Ochterski, R. L. Martin, K. Morokuma, V. G. Zakrzewski, G. A. Voth, P. Salvador, J. J. Dannenberg, S. Dapprich, A. D. Daniels, O. Farkas, J. B. Foresman, J. V. Ortiz, J. Cioslowski and D. J. Fox, *Gaussian 09 Revision B.01*, Gaussian Inc. Wallingford CT 2009.
19 E. Cancès, B. Mennucci and J. Tomasi, *J. Chem. Phys.*, 1997, **107**, 3032–3041.
20 K. Wolinski, J. F. Hinton and P. Pulay, *J. Am. Chem. Soc.*, 1990, **112**, 8251–8260.
21 T. Helgaker, M. Watson and N. C. Handy, *J. Chem. Phys.*, 2000, **113**, 9402–9409.
22 P. J. Flory, *Statistical Mechanics of Chain Molecules*, Wiley & Sons, New York, 1969.
23 *IUPAC. Compendium of Chemical Terminology, 2nd ed. (the "Gold Book")*, ed. A. D. McNaught and A. Wilkinson, Blackwell Scientific Publications, Oxford, UK, 1997.
24 Y. Sasanuma, H. Ohta, I. Touma, H. Matoba, Y. Hayashi and A. Kaito, *Macromolecules*, 2002, **35**, 3748–3761.
25 P. J. Flory, *Principles of Polymer Chemistry*, Cornell University Press, Ithaca, 1953.
26 S. Deguire and F. Brisse, *Can. J. Chem.*, 1988, **66**, 341–347.
27 D. Abe, Y. Sasanuma and H. Sato, *Acta Crystallogr., Sect. E: Struct. Rep. Online*, 2011, **67**, o961.
28 D. Abe and Y. Sasanuma, *Acta Crystallogr., Sect. E: Struct. Rep. Online*, 2013, **69**, o1612.
29 D. Abe and Y. Sasanuma, *Acta Crystallogr., Sect. E: Struct. Rep. Online*, 2013, **69**, o1636.
30 Y. Sasanuma, T. Ono, Y. Kuroda, E. Miyazaki, K. Hikino, J. Arou, K. Nakata, H. Inaba, K. ichi Tozaki, H. Hayashi and K. Yamaguchi, *J. Phys. Chem. B,*, 2004, **108**, 13163–13176.
31 P. J. Flory, *J. Chem. Phys.*, 1944, **12**, 425–438.
32 A. Asano and K. Takegoshi, *J. Chem. Phys.*, 2001, **115**, 8665–8669.

Table of contents entry Aromatic polythioesters and polydithioesters with different number of methylene units have been synthesized and characterized in terms of solubility, crystallinity, glass transition, melting, thermal decomposition, molecular motion, and thermal transition.